AIAA JOURNAL
Vol. 37, No. 11, November 1999

Conditional Analysis of Wall Pressure Fluctuations in Plume-Induced Separated Flowfields

R. J. Shaw*
SY Technology, Inc., Huntsville, Alabama 35806
and
J. C. Dutton† and A. L. Addy‡
University of Illinois at Urbana–Champaign, Urbana, Illinois 61801

The separation process in plume-induced, boundary-layer separated flowfields was found to be unsteady. Two in situ, fast-response pressure transducers were used to make individually and simultaneously sampled wall pressure fluctuation measurements over the intermittent region of separation shock wave motion. A conditional analysis technique was applied to the pressure–time histories, and statistical methods were then used to analyze the period, frequency, and velocity ensembles of the shock motion. The mean frequencies of this motion ranged between 1300 and 1500 Hz over the intermittent region, and the most probable shock wave frequencies occurred between 1 and 4 kHz over this region. The maximum zero-crossing frequency of the shock wave motion was approximately 500–600 Hz. The mean (approximately 3.5% of the freestream velocity) and most probable (approximately 6% of the freestream velocity) shock wave velocities in either direction were found to be essentially constant over the intermittent region. These results are compared to those for shock wave/boundary-layer interactions caused by solid protruberances.

Introduction

PLUME-INDUCED boundary-layer separation (PIBLS) is an important phenomenon that can adversely affect the aerodynamic and heat transfer characteristics of rockets and missiles. It occurs when the blockage caused by a highly underexpanded jet plume causes the afterbody boundary layer to separate upstream of the base corner. The only known previous investigations of the separation shock dynamics in a PIBLS flow utilized a cone–cylinder model that was wall mounted in a supersonic ($M = 2.5$–3.5) wind tunnel.[1–3] A secondary air jet at Mach 2.94 was injected into the freestream at a 74-deg angle with respect to the model axis near the aft end. Schlieren movies showed the length of the intermittent region associated with the separation shock motion to be on the order of a few boundary-layer thicknesses. Limited time-series analyses of measurements made with a sparsely distributed set of fast-response pressure transducers were performed. A power spectrum computed from one pressure–time history showed that most of the energy of the pressure fluctuations associated with the shock motion was contained below 1 kHz. No conditional analyses of the pressure fluctuation measurements were reported.

Our studies in a supersonic wind-tunnel facility used to produce PIBLS have also shown the separation process to be unsteady.[4,5] The separation shock wave was observed to translate randomly in the streamwise direction over a distance of several incoming boundary-layer thicknesses. Wall static pressure fluctuation measurements were made in the intermittent region using two flush-mounted, fast-response pressure transducers. Standard time-series analysis techniques were applied to the pressure–time histories obtained from these pressure transducers, and the resulting statistical properties were used to characterize the separation shock wave motion.[5] However, because each pressure–time history obtained from the intermittent region contains pressure fluctuations caused by the shock wave motion, as well as pressure fluctuations caused by turbulence in both the incoming boundary layer and the downstream separated region, it can be difficult to differentiate between effects caused by these two pressure fluctuation sources. In fact, the turbulence pressure fluctuations can entirely mask the effect of shock motion pressure fluctuations in some statistical properties. For example, the convection velocities of the shock wave motion could not be calculated from cross-correlation estimates because no convection times corresponding to the shock wave motions were found to exist in these estimates.[4] To isolate the pressure fluctuations caused by the shock motion from those caused by turbulence and then to analyze only those pressure fluctuations caused by the shock motion, a conditional analysis algorithm was applied to the pressure–time histories. The results obtained from conditionally analyzing the pressure fluctuation measurements made across the intermittent region of PIBLS flowfields are the subject of this paper.

The conditional analysis algorithm employed was the two-threshold method box-car conversion technique (TTMBCC) that has been developed by Dolling and Narlo,[6] Brusniak,[7] Dolling and Brusniak,[8] and Erengil and Dolling.[9] The TTMBCC algorithm has been used to successfully calculate the unsteady characteristics of the separation shock wave motion in several shock wave/turbulent boundary-layer interaction (SWBLI) flowfields produced by solid protuberances. Specifically, the zero-crossing frequency distributions across the intermittent region and the probability density function (PDF) estimates of the periods, frequencies, and velocities of the shock wave motions across the intermittent region have been calculated from pressure fluctuation measurements made in flowfields produced by compression ramps,[9,10] circular cylinders,[11] and hemicylindrical blunt fins.[12,13]

These studies have shown that the zero-crossing frequency f_c, i.e., the average number of times per second that the shock wave unidirectionally crosses a pressure transducer, along the line of symmetry upstream of the cylinders and fins appeared to be distributed parabolically over the length of the intermittent region and reached a maximum value near an intermittency of 50%. For the circular cylinders,[11] $f_{c,\max}$ ranged between 0.9 and 1.6 kHz, depending on the incoming boundary-layer thickness and the cylinder diameter. The trends exhibited by $f_{c,\max}$ for various cylinder diameters and boundary-layer thicknesses were the same trends displayed by the dominant center frequency in the power spectral density (PSD) estimates. For the swept hemicylindrical blunt fin experiments,[12] $f_{c,\max}$ ranged from 1.2 to 2.2 kHz as the leading-edge sweep angle increased from 0 to 45 deg. A PDF estimate of the shock wave periods

Received 11 August 1998; revision received 12 March 1999; accepted for publication 30 March 1999.

*Research Engineer.

†W. Grafton and Lillian B. Wilkins Professor, Department of Mechanical and Industrial Engineering.

‡Professor Emeritus, Department of Mechanical and Industrial Engineering.

at each location across the intermittent region showed that all of the distributions of shock wave periods were strongly skewed toward shorter periods. The most probable period, which occurred somewhere over the 0.2–0.5 ms range, depending on the intermittency, was always less than the mean period for each distribution. Similarly, PDF estimates of the shock wave frequencies have shown that, although frequencies as high as 10 kHz exist in the distributions, the most probable shock wave frequencies were in the 1–2 kHz range.[11]

From the ensembles of shock wave velocities calculated with the TTMBCC algorithm applied to swept hemicylindrical blunt fin, sharp fin, and swept compression ramp interactions, the mean and rms of the shock wave velocities, when nondimensionalized by the freestream velocity, were found to be independent of the geometry that produced the interaction and independent of the intermittent region length.[13] This result explained the inverse relationship between the length of the intermittent region and the zero-crossing frequency that was observed in several experiments. The average mean and rms of the shock wave velocities for these interactions were calculated to be $0.0304U_\infty$ and $0.0055U_\infty$, respectively, in the upstream direction and $0.0310U_\infty$ and $0.0056U_\infty$, respectively, in the downstream direction, where U_∞ is the freestream velocity approaching the fin or ramp.

The investigations just mentioned have shown that conditional analysis of pressure–time histories obtained from SWBLIs produced by solid protuberances has been beneficial primarily in determining the unsteady characteristics of the separation shock wave motions. By applying both standard time-series analysis and conditional analysis techniques to the pressure–time histories obtained from SWBLIs, a more complete picture of the shock wave motion was obtained for solid boundary protuberances. By applying both analysis techniques in the present PIBLS flowfield study, a more complete picture of the shock wave motion is also obtained for separation caused by a compliant aerodynamic boundary. The time-series results for the PIBLS flow have previously been presented in Ref. 5; the conditional analysis measurements are presented and discussed herein.

Experimental Equipment and Procedure

Wind-Tunnel Facility

The experiments were conducted in a supersonic flow facility designed specifically to produce PIBLS flowfields. Figure 1 presents a schematic of the flow facility and a cross-sectional view of the test section. PIBLS of the upper $M = 2.5$ stream is caused by impinging it at a 40-deg angle, across a 12.7-mm base height, with the lower $M = 1.5$ stream. The test section is two dimensional with a constant width of 50.8 mm. The height of the $M = 2.5$ stream is also 50.8 mm. Glass window assemblies are installed in each sidewall, allowing optical access to the entire PIBLS flow interaction.

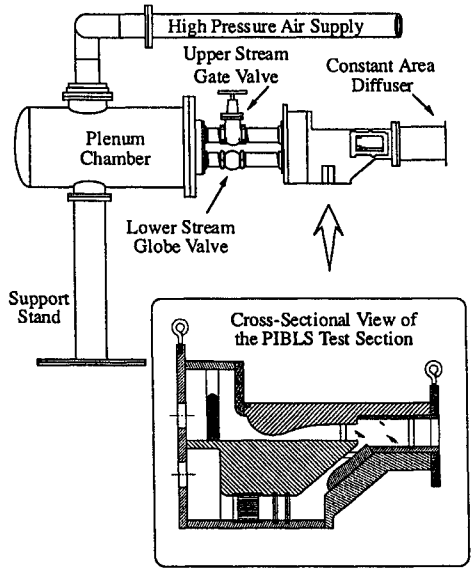

Fig. 1 Schematic of the flow facility and PIBLS test section.

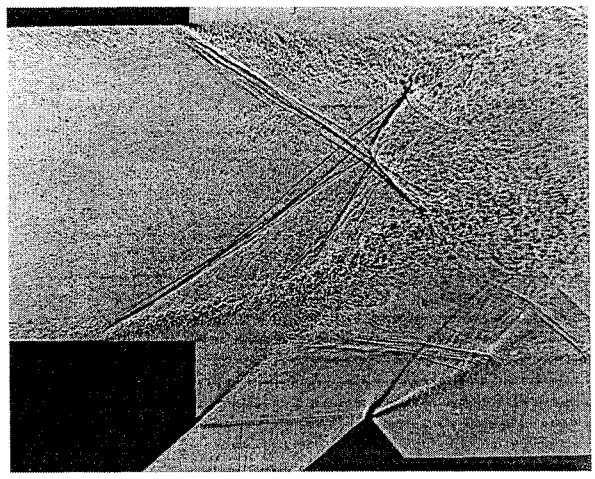

Fig. 2 Shadowgraph photograph (flashlamp pulse duration of 25 ns) of the near-wake region in the PIBLS wind tunnel at a JSPR of approximately 2.35.

Filtered, dry air was supplied to the test section via two screw compressors and air storage tanks. Flow conditioning screens and honeycomb sections were installed in the supply lines of both streams. In addition, the lower stream could be throttled using a manual valve. Varying the lower stream stagnation pressure in this way was used to adjust the jet static pressure ratio $[(\text{JSPR}) = P_{\text{lower}}/P_{\text{upper}}]$ between the two streams and, therefore, the mean separation location of the boundary layer of the upper stream.

Figure 2 is a shadowgraph photograph of the PIBLS flowfield taken at JSPR = 2.35. Plume-induced separation of the upper stream's boundary layer and the separation shock wave are clearly visible. When the shadowgraph light source was operated continuously, the separation shock was observed to experience unsteady streamwise motions at all JSPRs considered. Also visible in Fig. 2 are the separated shear layers from both streams, the enclosed recirculation region, the recompression waves near the shear layer reattachment point, and the trailing wake.

Surface oil-streak visualizations (not shown here) confirmed, at least in a mean sense, that there is little or no spanwise variation in the separation process of the Mach 2.5 stream over the inner 60% or so of the flow away from the wind-tunnel walls.

Instrumentation

Wall pressure fluctuations in the neighborhood of the separation location were measured with two Kulite® piezoresistive pressure transducers flush mounted in the upper wall of the center partition (Fig. 1). The upstream and downstream transducers were located 19.1 and 16.5 mm upstream of the base, respectively, on the spanwise center plane of the test section. The transducer diaphragms had an active diameter of 0.71 mm and measured diaphragm natural frequencies of 168 and 198 kHz for the upstream and downstream transducers, respectively. The transducers were statically calibrated in situ using a Sensotec digital pressure gauge that is accurate to within ±103 Pa. Amplification of the analog voltage signal from the transducers was carried out with a Measurements Group® signal conditioning amplifier. Low-pass filtering of the amplified signals was performed with an active Butterworth filter circuit. The low-pass filters had a −3-dB cutoff frequency of 50 kHz and an attenuation of −36 dB/octave in the transition band. The gain and dc offset of each channel were adjusted before each calibration to maximize the signal-to-noise ratio (SNR) of the output signal. The resulting SNRs for the fluctuating pressure measurements were in the range of 15–20 for the incoming boundary layer and from 55–300 for the intermittent region.

Data Acquisition

In these experiments the two Kulite pressure transducers were mounted at fixed positions on the center partition. As a result, the shock wave intermittent region was moved across the transducer locations by varying the JSPR. Specifically, the shock wave

intermittency (fraction of time the shock is upstream of a transducer) was increased by increasing the lower jet stagnation pressure, and therefore the JSPR, from 210 to 269 kPa in increments of approximately 3.4 kPa. Variation in the location of these two transducers, or use of additional transducers, was not possible due to the relatively small size of the center partition (Fig. 1) where the transducers were located.

Both individually and simultaneously sampled pressure measurements were obtained at each JSPR. The individually sampled measurements were made at a rate of 166,667 samples/s for 24 s for each transducer. The simultaneously sampled transducer readings were obtained at 200,000 samples/s per channel for 20 s.

Further details concerning the flow facility, instrumentation, and data acquisition methods may be found in Refs. 4 and 5.

Analysis Technique

The updated version[9] of the TTMBCC algorithm, developed in Refs. 6–9, was used in the analysis of the shock motion of the PIBLS flowfield. In this method each individual pressure measurement from a given transducer is compared to two threshold levels, Th_1 and Th_2, and the instantaneous shock location is then determined as either upstream or downstream of the transducer. The precise time (to within the sampling period) at which the shock crosses upstream of the transducer, called the rise time, and downstream of the transducer, called the fall time, is determined for all shock passages in the time history of the pressure measurements. The resulting record of the shock rise and fall times is the box-car function.

An analysis of the TTMBCC algorithm was performed with the PIBLS data to evaluate the sensitivity of the zero-crossing frequency f_c to different threshold settings. Two discrete settings of Th_1 were used in the sensitivity analysis: $Th_1 = \bar{p}_{w0}$ and $\bar{p}_{w0} + 3\sigma_{p_{w0}}$, where $\bar{p}_{w0}$ is the mean pressure and $\sigma_{p_{w0}}$ is the rms of the pressure fluctuations in the incoming boundary layer. For each of the two Th_1 settings, threshold level Th_2 was systematically varied according to $Th_2 = \bar{p}_{w0} + n\sigma_{p_{w0}}$, where n is an integer in the range $3 \leq n \leq 9$. For each of two pressure–time histories ($\gamma \approx 20$ and 50%), the TTMBCC algorithm was used to calculate f_c at each of the 14 unique combinations of Th_1 and Th_2. The results are shown in Fig. 3. Three main observations may be made about the sensitivity of f_c to the two threshold levels: 1) f_c decreased as threshold level Th_2 increased (larger n values) at both intermittencies regardless of the setting for Th_1, 2) f_c was larger for $Th_1 = \bar{p}_{w0} + 3\sigma_{p_{w0}}$ than for $Th_1 = \bar{p}_{w0}$ at both intermittencies regardless of the setting for Th_2, and 3) f_c was more sensitive to the threshold level settings at $\gamma \approx 50\%$ than at $\gamma \approx 20\%$. The first two observations are obvious from Fig. 3, but the last one required a separate, quantitative study,[4] whose results are not shown here for conciseness. Because the sensitivity analysis performed on the PIBLS data showed similar, albeit weaker, qualitative trends when compared to the sensitivity analysis performed on the Mach 5 circular cylinder interaction data,[8] it was concluded that threshold level settings of $Th_1 = \bar{p}_{w0} + 3\sigma_{p_{w0}}$ and $Th_2 = \bar{p}_{w0} + 6\sigma_{p_{w0}}$ were also reasonable choices for conditional analysis of the PIBLS data.

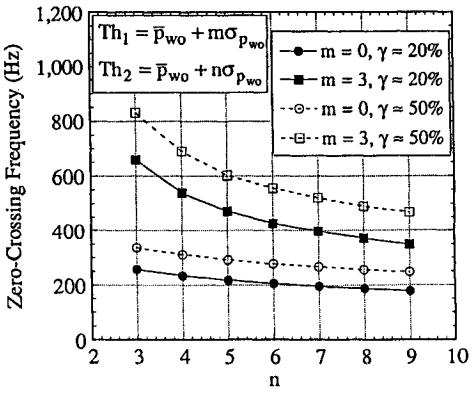

Fig. 3 Sensitivity of the zero-crossing frequency to the threshold levels in the TTMBCC algorithm for the PIBLS experiments.

Results

After specifying the flow conditions for the experiments, results from the pressure transducer measurements will be presented in two parts: individually sampled transducer measurements and simultaneously sampled transducer measurements. The individually sampled results were used to calculate period and frequency ensembles of the shock wave motion, and the simultaneously sampled data were used to calculate velocity ensembles of the shock motion.

Flow Conditions

The stagnation temperature of both streams was measured with an iron–constantan thermocouple mounted in the facility plenum chamber and was found to be 298 K (±1.5 K). The stagnation pressure of each stream was measured with a probe mounted upstream of each nozzle block. The stagnation pressure of the upper stream was 503 kPa (±1.5 kPa), and its unit Reynolds number was $47.1 \times 10^6\ \mathrm{m}^{-1}$ ($\pm 0.5 \times 10^6\ \mathrm{m}^{-1}$). The Mach number of this freestream was determined from the stagnation pressure measurement and mean static pressure measurements made using taps located in the center partition and was found to be 2.50 (±0.01). The Mach number of the lower jet was determined in a similar manner to be 1.51 (±0.01).

Velocity measurements were made in the upper stream along a vertical traverse 30 mm upstream of the base using a one-component laser Doppler velocimeter setup. The freestream turbulence intensity was found to be less than 0.015 (±0.0015) across the uniform portion of the mean profile. A wall-wake velocity profile of the form suggested by Sun and Childs[14] was curve fit to the mean velocity measurements made in the boundary layer, and from this fit the integral boundary-layer parameters were determined (Table 1). These parameters agree well with those of other equilibrium turbulent boundary layers reported in the literature[15–17] for comparable Reynolds and Mach numbers.

Individually Sampled Pressure Transducer Measurements

Although the JSPR was the independent variable in the experiments, some results will be presented as a function of intermittency rather than JSPR. As mentioned earlier, intermittency γ is defined as the percentage of time the shock wave is upstream of a given pressure transducer and is calculated from

$$\gamma = \frac{\sum_{k=1}^{N} (\mathrm{fall}_k - \mathrm{rise}_k)}{\mathrm{fall}_N - \mathrm{rise}_1} \tag{1}$$

where fall_k is the fall time associated with the kth downstream shock wave crossing, rise_k is the rise time associated with the kth upstream shock crossing, and N is the total number of fall times detected in the pressure–time history.

A plot of intermittency vs JSPR over the intermittent region is shown in Fig. 4 for both the upstream and downstream transducers. For the downstream transducer measurements, the JSPR range from 1.95 to 2.41 spanned the intermittency range from $\gamma = 3.9$ to 96.2%. Similarly, the upstream transducer measurements spanned the intermittent region from $\gamma = 3.8$ to 98.3% over a range of JSPR from 2.05 to 2.49. Over this range of downstream transducer intermittencies, the shock strength, as judged by its static pressure ratio, varied by only ±5% about its nominal value of 2.11. Also, with the intermittent region length defined to exist between the $\gamma = 4$ and 96% locations, the length of the intermittent region was estimated to be $2.6\delta_0$–$3.0\delta_0$ at JSPR = 1.95 and $5.4\delta_0$–$5.5\delta_0$ at JSPR = 2.41, where $\delta_0 = 3.1$ mm.

Table 1 Incoming turbulent boundary-layer properties in the upper stream

Property	Value
Boundary-layer thickness, δ	3.1 mm
Boundary-layer displacement thickness, δ^*	0.91 mm
Boundary-layer momentum thickness, θ	0.25 mm
Boundary-layer shape factor, $H = \delta^*/\theta$	3.71
Wake strength parameter, Π	1.58
Skin friction coefficient, C_f	0.00131
Friction velocity, u_τ	20.6 m/s

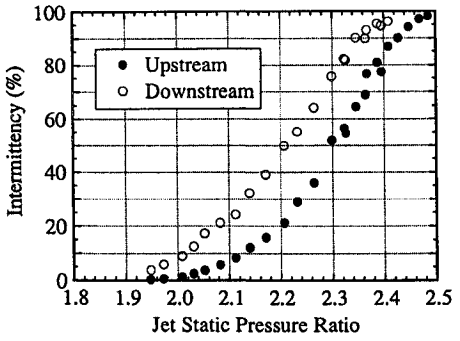

Fig. 4 Intermittency vs JSPR for the upstream and downstream pressure transducer measurements.

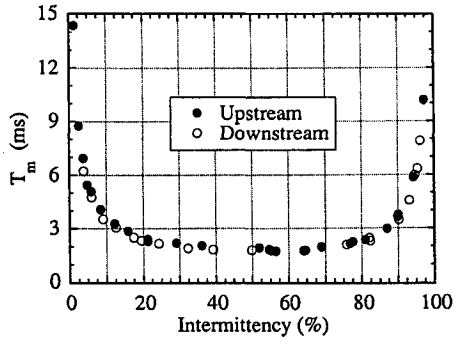

Fig. 5 Mean period of the shock wave motion vs intermittency across the intermittent region of PIBLS flowfields.

Periods of the Shock Wave Motion

The period of the ith shock wave event T_i in the box-car function can be calculated as the difference between two consecutive rise times ($T_i = \text{rise}_{i+1} - \text{rise}_i$) or the difference between two consecutive fall times ($T_i = \text{fall}_{i+1} - \text{fall}_i$). For both cases, statistical techniques can be applied to the ensemble of periods calculated from the box-car function to obtain the mean value, T_m, and the PDF of the ensemble. The distribution of mean periods over the intermittent region is shown in Fig. 5 for the upstream and downstream pressure transducer measurements. At every discrete intermittency at which experimental measurements were acquired, the mean period calculated from the rise times was equal (to three significant figures) to the mean period calculated from the fall times. As shown in Fig. 5, the mean periods computed from the upstream pressure transducer measurements also collapse on those determined from the downstream transducer measurements when the data are plotted vs intermittency. Although the mean period reached relatively large values at both low and high intermittencies, the value of the mean period decreased rapidly and was relatively constant as the midrange of intermittencies ($20\% < \gamma < 80\%$) was approached from both the low and high ranges. The distribution of mean periods reached a minimum value at $\gamma \approx 60\%$ where the mean period was in the range of 1.74–1.78 ms.

The PDF estimates of the shock wave periods were also computed across the intermittent region using both rise times and fall times. At each location over the intermittent region, the PDF estimate of the shock wave periods computed using rise times was essentially identical in shape and magnitude to that computed using fall times. This was the case for the upstream pressure transducer measurements as well as for the downstream transducer measurements. Because the evolution (in terms of the shape and magnitude) of these PDF estimates over the intermittent region was similar for both transducers, only the PDF estimates of the shock wave periods computed using the rise times from the downstream transducer measurements are shown in Fig. 6. The PDF estimates of the shock wave periods computed at five approximately equally spaced values across the intermittency range are shown in Fig. 6. Each of the PDF estimates is plotted in terms of $N_i/(N_{\text{total}}W)$ vs the shock wave period, where N_i is the number of shock wave periods occurring with a value of T_i, N_{total} is the total number of shock wave period realizations in the box-car function, and W is the interval width of the PDF estimate centered at T_i ($W = 36\,\mu$s). The mean period of each ensemble is also shown (with a solid black triangle) in each plot of Fig. 6.

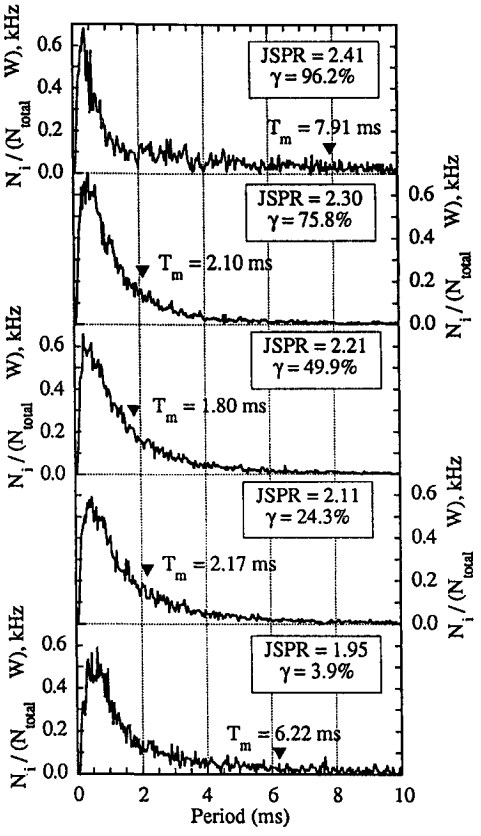

Fig. 6 PDF estimates of the shock wave periods at discrete locations across the intermittent region.

The behavior of the PDF estimates of the shock wave periods was similar over the entire intermittent region of the PIBLS flowfields. For each intermittency, the PDF quickly reached a maximum value at approximately 0.4 ms and then slowly decayed back to zero over the next 10–20 ms, depending on the intermittency. Over the low, e.g., $\gamma = 3.9\%$, and high, e.g., $\gamma = 96.2\%$, intermittency ranges, a number of shock wave events had periods longer than 10 ms, as evidenced by the amplitude of the PDF not being zero at 10 ms. Over the midrange of the intermittent region ($20\% < \gamma < 80\%$), nearly all of the individual shock wave periods were less than 10 ms. This trend explained the behavior of the mean period over the intermittent region. For the low and high intermittencies, the number of shock wave events with periods longer than 10 ms was sufficient to significantly increase the mean period to values well above (at least two or three times larger) those found over the midrange of the intermittent region.

Frequencies of the Shock Wave Motion

The frequency of the ith shock wave event, f_i, in the box-car function is simply the reciprocal of the period of the ith shock wave event, $f_i = 1/T_i$, and can be calculated from two consecutive rise times ($f_i = \{\text{rise}_{i+1} - \text{rise}_i\}^{-1}$) or from two consecutive fall times ($f_i = \{\text{fall}_{i+1} - \text{fall}_i\}^{-1}$). For both cases, statistical techniques can be applied to the ensemble of frequencies calculated from the box-car function to obtain the mean value f_m and the PDF of the ensemble. The distribution of mean frequencies over the intermittent region is shown in Fig. 7 and was calculated using the rise times from the upstream and downstream transducer measurements. The mean frequency calculated from the rise times was slightly larger than that calculated from the fall times at every measurement location over the intermittent region and for both the upstream and downstream transducer measurements. Thus, the mean frequency was more sensitive than the mean period to temporal differences between the rise times and the fall times. From Fig. 7, it is seen that the mean frequencies calculated using the upstream transducer measurements

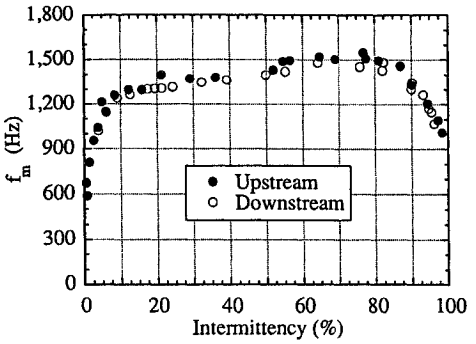

Fig. 7 Mean frequency of the shock wave motion vs intermittency across the intermittent region of PIBLS flowfields.

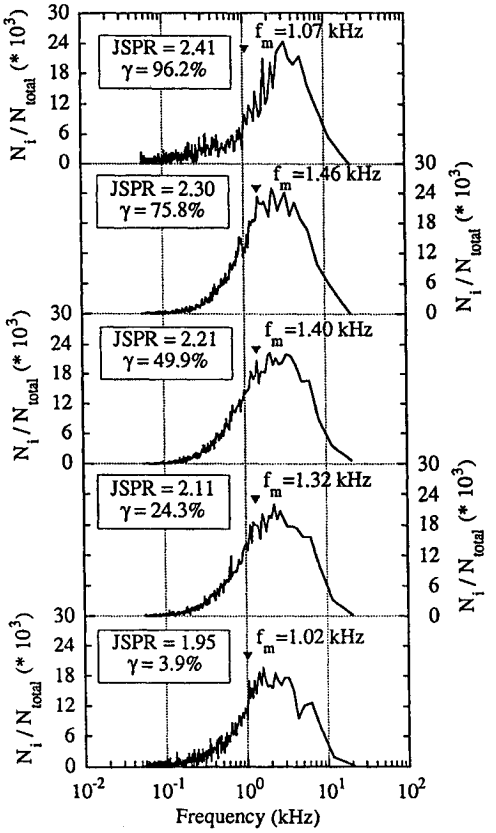

Fig. 8 PDF estimates of the shock wave frequencies at discrete locations across the intermittent region.

collapse on those calculated from the downstream transducer measurements when the frequency data are plotted vs intermittency. The mean frequencies ranged between 1300 and 1400 Hz over the intermittent region from 20 to 50% and between 1400 and 1500 Hz over the intermittent region from 50 to 80%.

PDF estimates of the shock wave frequencies were made at each measurement location across the intermittent region using both rise times and fall times. At each location, the PDF computed using rise times was nearly identical in shape and magnitude to that computed using fall times. This was true for the upstream transducer measurements as well as for the downstream transducer measurements. Because the evolution of the PDF estimates of the shock wave frequencies over the intermittent region was similar for both transducers, only the PDFs of the shock wave frequencies computed using rise times from the downstream transducer measurements are shown in Fig. 8.

The PDF estimates of the shock wave frequencies computed at the same five locations over the intermittent region as the shock wave period PDFs (shown earlier in Fig. 6) are presented in Fig. 8. Because the interval width of each PDF estimate, W_{f_i}, was variable over the frequency spectrum, each PDF estimate was reported as a simple histogram to eliminate the bias caused by W_{f_i} on the magnitude of the PDF estimate. Each PDF is plotted as N_i/N_{total} vs the shock wave frequency, where N_i is the number of shock wave frequency realizations occurring with a value of f_i and N_{total} is the total number of shock wave frequency realizations in the box-car function. The mean frequency of each ensemble is also shown (with a solid black triangle) in each plot of Fig. 8. The behavior of the shock wave frequency PDFs was similar at all five locations over the intermittent region. The amplitude of the PDF increased substantially over the frequency range between 100 Hz and 1 kHz, reached a most probable value between 1 and 4 kHz, and then decreased back to zero again near 20 kHz. The mean frequency of each ensemble was less than the most probable frequency.

Because the frequencies in each PDF estimate were narrowly spaced over the low-frequency range and widely spaced over the high-frequency range, a probability distribution function estimate was calculated for each PDF to better interpret the evolution of the PDFs over the intermittent region. When the PDF is defined as a simple histogram, the probability distribution function is the running sum of the PDF over the frequency range. For each PDF estimate shown in Fig. 8, a probability distribution function estimate was computed from

$$P_i = \sum_{j=1}^{i} N_j / N_{\text{total}} \tag{2}$$

where P_i is the probability distribution function corresponding to f_i. The probability distribution function estimates of the shock wave frequencies are shown in Fig. 9. The relative number of

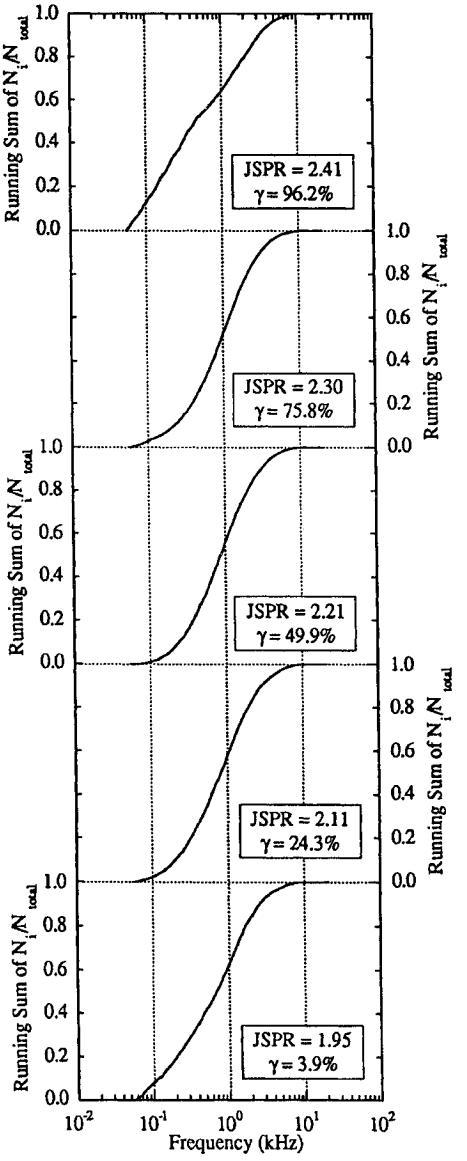

Fig. 9 Probability distribution function estimates of the shock wave frequencies at discrete locations across the intermittent region.

frequency realizations that occurred between 50 Hz and 1 kHz decreased, whereas the relative number of frequency realizations that occurred between 1 and 10 kHz increased as the $\gamma = 70\%$ location was approached from both the low and high intermittency ranges. Therefore, the individual frequency realizations in the ensembles occurred at higher frequencies as the $\gamma = 70\%$ location was approached. This trend explained why the mean frequency increased as the $\gamma = 70\%$ location was approached from the low and high intermittency ranges.

It is interesting to compare the PSD estimates of the pressure fluctuations computed from the pressure–time histories over the intermittent region[5] to the PDF and probability distribution function estimates computed from the ensembles of shock wave frequencies. The PSD estimates showed that 50–60% of the energy in the pressure fluctuations occurred between approximately 50 Hz and 1 kHz. The probability distribution function estimates of the shock wave frequencies showed that 50–60% of the shock wave events occurred over this same frequency range. Thus, more than half of the shock wave events, which contained more than half of the energy in the power spectrum, occurred at frequencies in this range. The PSD estimates showed that the energy in the pressure fluctuations dropped off significantly at frequencies higher than 1 kHz. Although only 15–30% of the energy in the PSD estimates was contributed by pressure fluctuations in the frequency range between 1 and 10 kHz, 40–50% of all of the shock wave frequencies occurred in this range, including the most probable shock wave frequencies. Therefore, the most probable shock wave frequencies (in the 1–4 kHz range) were not the most energetic frequencies (usually below 1 kHz).

The mean frequency over the intermittent region is not the only frequency that can be calculated for the shock wave motion. The zero-crossing frequency of the shock wave motion, computed as the reciprocal of the mean period, is also of interest. The distribution of the zero-crossing frequency over the intermittent region is shown in Fig. 10 for both the upstream and downstream pressure transducer measurements. The zero-crossing frequency distribution for the downstream transducer measurements reached a maximum of 560 Hz at $\gamma \approx 60\%$. The zero-crossing frequency distribution for the upstream pressure transducer measurements displayed an unusual 50-Hz shift near $\gamma \approx 50\%$, which was caused by a leak in the sidewall seal during the latter phases of the experiments.[4] Had the rupture not occurred, the upstream pressure transducer measurements would have reached a maximum of about 520 Hz at $\gamma \approx 60\%$. Note that the maximum zero-crossing frequency computed from the downstream pressure transducer measurements was larger than that computed from the upstream pressure transducer measurements. The physical reason for this will become clear after discussing the shock wave velocity distributions in the next section.

Simultaneously Sampled Pressure Transducer Measurements

Because the cross-correlation estimates computed for each pair of pressure–time histories acquired across the intermittent region did not detect the convection times corresponding to the shock wave motion in the upstream and downstream directions,[4,5] the convection time associated with each pair of shock wave crossings was computed from the conditional analysis of each pair of pressure–time histories. The TTMBCC algorithm was used to convert each pair of pressure–time histories into a pair of box-car functions. An ensemble of convection times for the shock wave motion in the upstream direction and an ensemble of convection times for motion in the downstream direction were formed at each JSPR by analyzing all of the pairs of shock wave crossings in the two box-car functions.[4] Assuming the shock wave moves with uniform speed and direction between the two pressure transducers, the velocities of the shock wave motion in the upstream and downstream directions were computed from the convection times between the two transducers and the transducer spacing.

The PDF estimates of the shock wave velocities in the upstream and downstream directions computed at five discrete locations over the intermittent region are shown in Figs. 11 and 12, respectively. Each of the PDFs is plotted as N_i/N_{total} vs $U_{\text{shock}}/U_\infty$, where N_i is the number of shock wave velocity realizations at velocity U_{shock}, N_{total} is the total number of realizations (in either direction) in each pair of box-car functions, and U_∞ is the freestream velocity of the Mach 2.5 flow (565 m/s). Whereas the behavior of the PDF estimates of the shock velocities in the upstream and downstream directions was similar over the intermittent region, the PDFs of the upstream shock velocity were less peaked and had a wider distribution than did those of the downstream shock velocity. As $U_{\text{shock}}/U_\infty$ increased, the PDF estimates quickly reached a maximum value over the velocity range of $0.04U_\infty$–$0.08U_\infty$ and then slowly decayed back to zero again by the time the shock wave velocity reached $0.30U_\infty$.

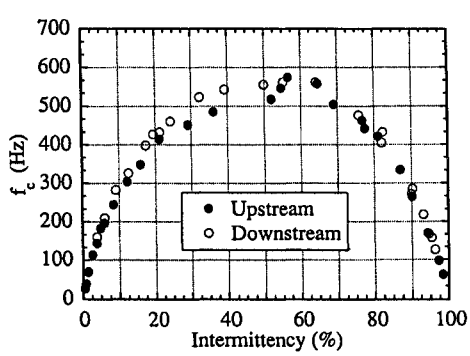

Fig. 10 Zero-crossing frequency of the shock wave motion vs intermittency across the intermittent region of PIBLS flowfields.

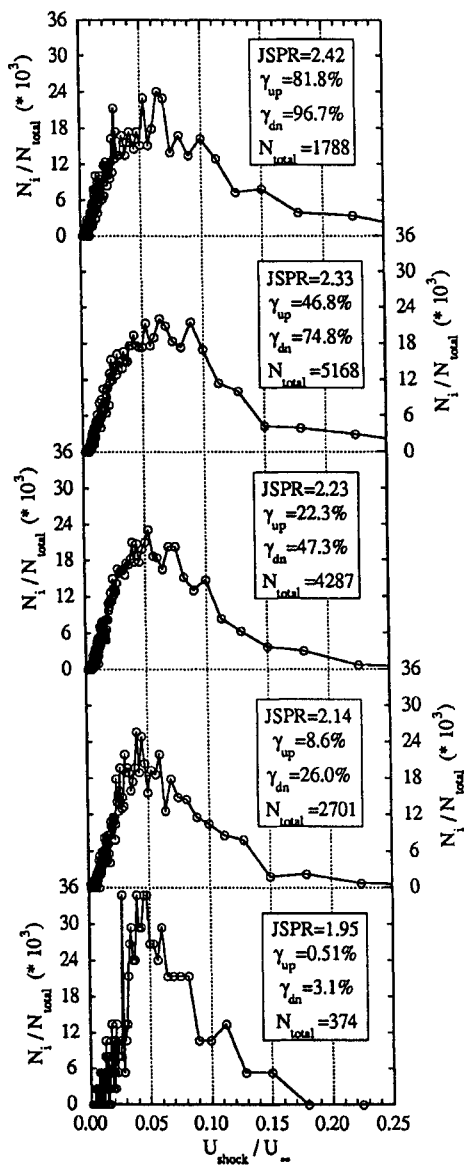

Fig. 11 PDFs of the shock wave velocity in the upstream direction across the intermittent region.

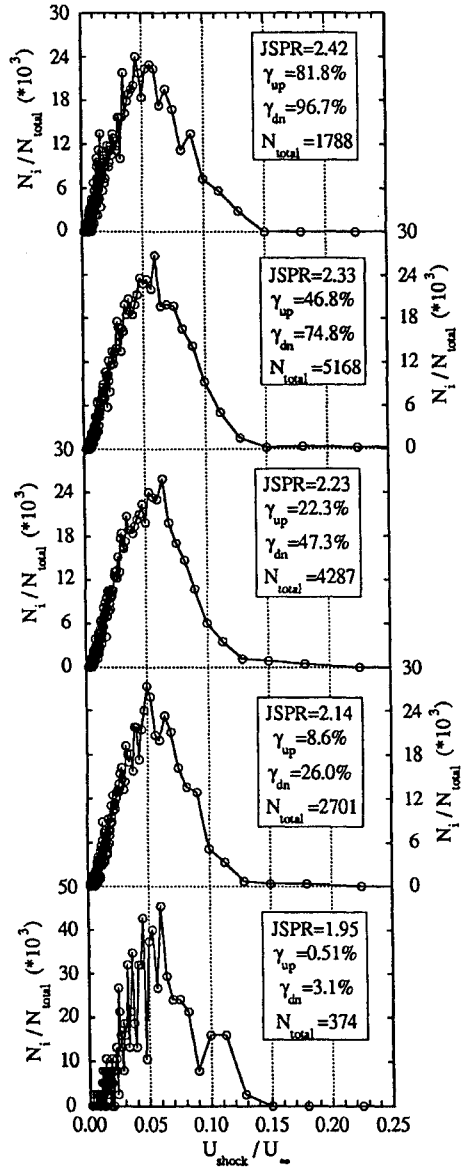

Fig. 12 PDFs of the shock wave velocity in the downstream direction across the intermittent region.

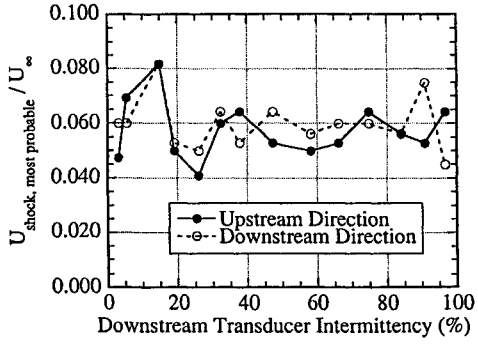

Fig. 13 Most probable shock wave velocity in the upstream and downstream directions across the intermittent region.

The most probable shock wave velocity in both the upstream and downstream directions was computed at 14 locations across the intermittent region and is shown in Fig. 13. The most probable shock wave velocity in either direction was essentially constant over the intermittent region. The average value of the most probable shock wave velocities was $0.058U_\infty \pm 0.010U_\infty$ in the upstream direction and $0.060U_\infty \pm 0.009U_\infty$ in the downstream direction and, thus, was essentially the same in the two directions.

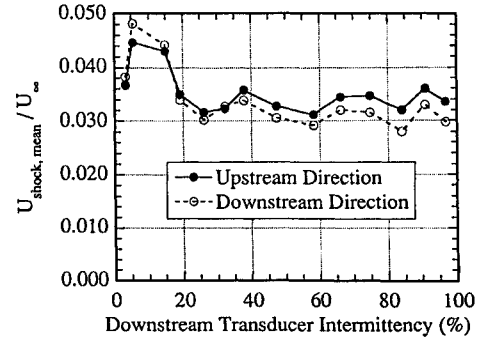

Fig. 14 Mean shock wave velocity in the upstream and downstream directions across the intermittent region.

The mean shock wave velocity in both the upstream and downstream directions was also computed at 14 locations across the intermittent region and is shown in Fig. 14. The mean shock wave velocity in either direction was fairly constant across the intermittent region. The average value of the mean shock wave velocity was $0.035U_\infty \pm 0.004U_\infty$ in the upstream direction and $0.034U_\infty \pm 0.006U_\infty$ in the downstream direction. Figure 14 shows that the mean shock wave velocity in the upstream direction was consistently slightly greater than the mean shock wave velocity in the downstream direction over most of the intermittent region. After a close examination of the threshold levels used in the TTMBCC algorithm to compute the shock wave velocities, the small differences between the mean shock wave velocities in the two directions that developed over the intermittent region was believed not to be an artifact of the conditional analysis technique, but rather was most likely caused by the physics of the shock wave motion. The trend of the mean shock wave velocity in the upstream direction being increasingly greater than the mean shock wave velocity in the downstream direction as the JSPR (and intermittency) increased was consistent with the trend observed in the PDF estimates of the shock wave velocities in the upstream and downstream directions. As the JSPR increased from 1.95 to 2.41 ($\gamma = 3.9$ to 96.2%), more shock wave velocity realizations with a magnitude larger than the most probable value occurred in the upstream direction than in the downstream direction.

The conditional analysis of the two simultaneously sampled pressure transducer measurements revealed that the average mean shock wave velocity in either direction was approximately $0.034U_\infty$–$0.035U_\infty$, and the mean shock wave velocity was independent of the intermittent region length. This explains why, for the same intermittency value, the zero-crossing frequency calculated from the pressure-time history acquired with the upstream pressure transducer was always less than the zero-crossing frequency calculated from the downstream transducer measurements. The length of the intermittent region increased from $2.6\delta_0$–$3.0\delta_0$ to 5.4–$5.5\delta_0$ (where δ_0 is the incoming boundary-layer thickness) as the JSPR increased from 1.95 to 2.49 (Ref. 4). For both pressure transducers to have the same intermittency value, the JSPR setting used for the upstream pressure transducer measurements was higher than that for the downstream transducer measurements. As a result, the intermittent region length associated with the upstream pressure transducer flowfield is longer than that for the downstream transducer measurement flowfield. Consequently, because the mean shock wave velocity is constant across the intermittent region, the zero-crossing frequency must be less for the upstream pressure transducer measurements than for the downstream transducer measurements.

Conclusion

Although the zero-crossing frequency and the mean frequency of the shock wave motion in the current PIBLS flowfields were less than the frequencies found in other SWBLIs produced by solid protuberances,[9–13] the velocity characteristics of the shock wave motion were similar to the velocity characteristics of the shock wave motion in solid protruberance SWBLI flowfields. These similarities included the general shape of the PDF estimates of the shock wave velocities, which were highly skewed toward low-speed realizations

relative to the freestream velocity, the most probable shock velocities of approximately $0.05U_\infty$–$0.10U_\infty$, and the average mean shock velocities of approximately $0.03U_\infty$. Although all of these similarities are undoubtedly important, the latter similarity is especially noteworthy. Gonsalez and Dolling[13] found that the average mean shock wave velocities in either direction were approximately $0.030U_\infty$–$0.031U_\infty$ and were independent of the intermittent region length for swept compression ramp interactions, hemicylindrical blunt fin interactions, and sharp fin interactions at angles of attack. The current PIBLS study found that the average mean shock wave velocity in either direction was approximately $0.034U_\infty$–$0.035U_\infty$ and that it was independent of the intermittent region length. Thus, the average mean shock wave velocities from the plume-induced interactions were essentially the same as the average mean shock wave velocities from the interactions produced by the three solid geometries.

Although there were many similarities between the velocity characteristics of the shock wave motion in the PIBLS flowfields and those in SWBLI flowfields produced by solid geometries, a difference found between the two types of interactions was that the upstream mean shock velocities were greater than the downstream mean shock velocities in the plume-induced interactions, whereas just the opposite situation was found in the solid geometry interactions.[9–13] A definitive explanation of this result must await further study.

Acknowledgments

The authors gratefully acknowledge the financial support of the U.S. Army Research Office under Grant DAAH04-93-G-0226 with Thomas L. Doligalski as Technical Monitor. The authors also thank David S. Dolling of the University of Texas at Austin for providing the code for the conditional analysis algorithm.

References

[1]Bogess, A. L., "An Investigation of the Unsteady Flow Associated with Plume Induced Flow Separation," Bureau of Engineering Research, Rept. 149-02, Univ. of Alabama, Tuscaloosa, AL, 1972.

[2]Doughty, J. O., "Effects of Periodic Plume Pulsing on the Flow Field Generated by Plume Induced Flow Separation," Bureau of Engineering Research, Rept. 164-02, Univ. of Alabama, Tuscaloosa, AL, 1973.

[3]Doughty, J. O., "A Study of a Plume Induced Separation Shock Wave, Including Effects of Periodic Plume Unsteadiness," Bureau of Engineering Research, Rept. 207-02, Univ. of Alabama, Tuscaloosa, AL, 1976.

[4]Shaw, R. J., "An Experimental Investigation of Unsteady Separation Shock Wave Motion in a Plume-Induced, Separated Flowfield," Ph.D. Dissertation, Dept. of Mechanical and Industrial Engineering, Univ. of Illinois, Urbana, IL, Aug. 1995.

[5]Shaw, R. J., Dutton, J. C., and Addy, A. L., "Time-Series Analyses of Wall Pressure Fluctuations in Plume-Induced Separated Flowfields," *AIAA Journal*, Vol. 36, No. 10, 1998, pp. 1817–1824.

[6]Dolling, D. S., and Narlo, J. C., "Driving Mechanism of Unsteady Separation Shock Motion in Hypersonic Interactive Flow," *Aerodynamics of Hypersonic Lifting Vehicles*, CP-428, AGARD, 1987, pp. 7-1–7-12.

[7]Brusniak, L., "Evaluation of Conditional Sampling Methods for Analysing Separation Shock Motion," AIAA Paper 88-0091, Jan. 1988.

[8]Dolling, D. S., and Brusniak, L., "Separation Shock Motion in Fin, Cylinder, and Compression Ramp-Induced Turbulent Interactions," *AIAA Journal*, Vol. 27, No. 6, 1989, pp. 734–742.

[9]Erengil, M. E., and Dolling, D. S., "Unsteady Wave Structure near Separation in a Mach 5 Compression Ramp Interaction," *AIAA Journal*, Vol. 29, No. 5, 1991, pp. 728–735.

[10]Dolling, D. S., Boitnott, T., and Erengil, M. E., "Effects of Moderate Sweepback on the Separation Shock Wave Dynamics in a Mach 5 Compression Ramp Interaction," AIAA Paper 91-0254, Jan. 1991.

[11]Dolling, D. S., and Smith, D. R., "Separation Shock Dynamics in Mach 5 Turbulent Interactions Induced by Cylinders," *AIAA Journal*, Vol. 27, No. 12, 1989, pp. 1698–1706.

[12]Kleifges, K., and Dolling, D. S., "Control of Unsteady Shock-Induced Turbulent Boundary Layer Separation Upstream of Blunt Fins," AIAA Paper 93-3281, July 1993.

[13]Gonsalez, J. C., and Dolling, D. S., "Correlation of Interaction Sweepback Effects on the Dynamics of Shock-Induced Turbulent Separation," AIAA Paper 93-0776, Jan. 1993.

[14]Sun, C. C., and Childs, M. E., "A Modified Wall Wake Velocity Profile for Turbulent Compressible Boundary Layers," *Journal of Aircraft*, Vol. 10, No. 6, 1973, pp. 381–383.

[15]Coles, D., "Measurements in a Flat Plate Boundary Layer at the Jet Propulsion Laboratory," Jet Propulsion Lab., Rept. 20-71, California Inst. of Technology, Pasadena, CA, 1953.

[16]Winter, K. G., and Gaudet, L., "Turbulent Boundary Layer Studies at High Reynolds Numbers at Mach Numbers Between 0.2 and 2.8," Aeronautical Research Council, Repts. and Memoranda 3712, London, 1973.

[17]Fernholz, H. H., and Finley, P. J., "A Critical Commentary on Mean Flow Data for Two-Dimensional Compressible Turbulent Boundary Layers," AGARDograph 253, May 1980.

M. Sichel
Associate Editor